JACS
JOURNAL OF THE AMERICAN CHEMICAL SOCIETY

ARTICLE

pubs.acs.org/JACS

# Purely Heterometallic Lanthanide(III) Macrocycles through Controlled Assembly of Disulfide Bonds for Dual Color Emission

David J. Lewis, Peter B. Glover, Melissa C. Solomons, and Zoe Pikramenou*

School of Chemistry, The University of Birmingham, Edgbaston B15 2TT, United Kingdom

Supporting Information

**ABSTRACT:** Lanthanide complexes based on bis(amides) of diethylenetriaminepentaacetic acid with thiol functionalities are modified with 2,2′-dipyridyl disulfide to give activated complexes that can selectively react with thiol-functionalized complexes to form heterometallic lanthanide macrocycles. The preparation and full characterization of the polyaminocarboxylate ligands *N*,*N*′′-bis-[*p*-thiophenyl(aminocarbonyl)]diethylenetriamine-*N*,*N*′,*N*′′-triacetic acid ($\mathbf{H_3L^x}$) and the activated *N*,*N*′′-bis[*p*-(pyridyldithio)-[phenyl(aminocarbonyl)]]diethylenetriamine-*N*,*N*′,*N*′′-triacetic acid ($\mathbf{H_3L^y}$) and the complexes $\mathbf{LaL^x}$, $\mathbf{NdL^x}$, $\mathbf{SmL^x}$, $\mathbf{EuL^x}$, $\mathbf{GdL^x}$, $\mathbf{DyL^x}$, $\mathbf{TbL^x}$, $\mathbf{ErL^x}$, and $\mathbf{YbL^x}$ are reported. The luminescence properties of the $\mathbf{LnL^x}$ complexes emitting in the visible (where Ln = $Dy^{3+}$, $Tb^{3+}$, $Eu^{3+}$, and $Sm^{3+}$) are examined by steady-state and time-resolved photoluminescence, and the triplet state energy level of $\mathbf{GdL^x}$ was estimated to be 24 100 $cm^{-1}$ from the *0*−0 band of the 77 K phosphorescence spectrum. Near-infrared emission was detected for the $\mathbf{NdL^x}$, $\mathbf{YbL^x}$, and $\mathbf{ErL^x}$ complexes, demonstrating the versatility of the thiophenol chromophore. The assembly of purely heterometallic $\mathbf{EuTbL^x_2}$ macrocycles by reaction of $\mathbf{EuL^x}$ with $\mathbf{TbL^y}$ was followed by UV−vis absorption spectroscopy, monitoring the characteristic absorption peak of pyridyl-2-thione at 353 nm. Analysis of the solution by mass spectrometry reveals the formation of purely heterometallic macrocycle $\mathbf{EuTbL^x_2}$. This is in contrast with the results obtained by dynamic self-assembly under oxidative conditions, where we observe a statistical mixture of macrocyclic complexes of $\mathbf{Eu_2L^x_2}$, $\mathbf{Tb_2L^x_2}$, and $\mathbf{EuTbL^x_2}$. The $\mathbf{EuTbL^x_2}$ macrocycle displays dual color emission, incorporating the characteristic *f*−*f* transitions of $Eu^{3+}$ and $Tb^{3+}$. Investigation into the time-resolved photophysical properties of $\mathbf{EuTbL^x_2}$ reveals energy transfer from $Tb^{3+}$ to $Eu^{3+}$, facilitated by the different conformations of the macrocycle in solution.

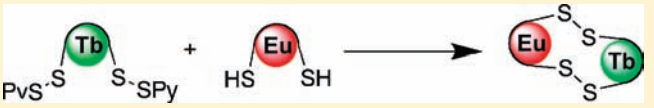


## INTRODUCTION

The design of multifunctional probes is important in molecular multimodal imaging applications where different detection techniques are employed to achieve high sensitivity and spatial resolution.[1] For example, recent advances highlight the dual detection advantages of employing a combination of magnetic resonance imaging (MRI) or X-ray techniques with luminescence to image cells.[2−5] Ratiometric luminescent probes that use different emission colors for analysis of complex biological samples are also widely used as an approach to multiple signal detection.[6,7] Ideally it is desirable that the output signals are generated by probes incorporated into a single molecular entity to achieve consistent, targeted delivery of the probe. Lanthanides are widely used as luminescent probes with the wavelength of the light emission to be determined by the choice of the lanthanide ion, whether it is a visible ($Sm^{3+}$, $Eu^{3+}$, $Tb^{3+}$, and $Dy^{3+}$) or near-infrared emitter ($Nd^{3+}$, $Er^{3+}$, and $Yb^{3+}$) and with large Stokes shift between excitation and emission light. The wide spectrum of emission and the narrow patterned spectra make them ideal candidates for ratiometric probes. Additionally, the coordination preferences of the emissive lanthanide ions are very similar to $Gd^{3+}$, which is known for its activity as a contrast agent in MRI. Heterometallic lanthanide complexes are therefore popular as they are potentially able to incorporate luminescent properties with magnetic ones by judicious choice of metal centers. However, due to their similar coordination preferences, it is a challenge to synthesize heterometallic complexes containing two or more different lanthanides, and many attempts using macrocyclic structures have led to statistical mixtures.[8,9]

The approaches for heterometallic complexes adopted to date[10−17] rely on either self-assembly by size selectivity of the lanthanides or on "statistical crystallisation". The first approach is based on appropriate ligand design with multidentate pockets that are commensurate with lanthanide size, while the second strategy relies on stepwise formation and reactions of stable complexes.

$\mathbf{H_3L^x}$ and $\mathbf{H_3L^y}$ (Scheme 1) were designed to provide a hard base binding core for lanthanide complexation, via three carboxylate and two amide oxygen donors and three backbone nitrogen donors. Two pendant amide arms provide versatile thiophenol groups for binding to soft metals or forming disulfide bonds. Previously, we have reported lanthanide complexes of functional DTPA-bis(amides) as luminescent sensors,[18] taking part in the self-assembled formation of dinuclear lanthanide complexes,[19] in assembly with platinum moieties,[20] and assembled on luminescent gold nanoparticles.[21]

In this paper we introduce an activated thiol approach in the thiol−disulfide exchange chemistry for the solution assembly of $\mathbf{LnLn'L^x_2}$ macrocycles. We report the synthesis and characterization

**Received:** October 12, 2010
**Published:** December 23, 2010





dx.doi.org/10.1021/ja109157g | *J. Am. Chem. Soc.* 2011, 133, 1033–1043

**Scheme 1. Structures of $H_3L^x$, $H_3L^y$, and $EuTbL^x_2$**

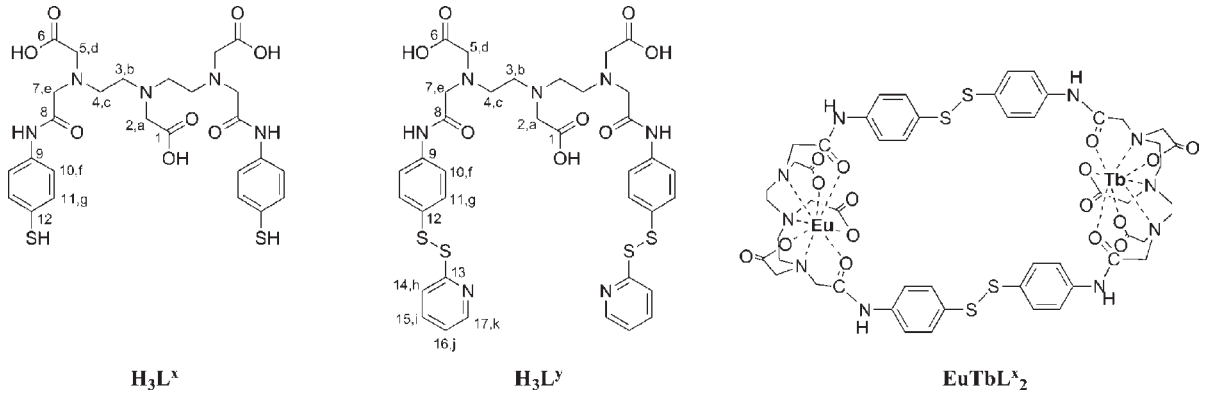


of $H_3L^x$, $H_3L^y$, and $LnL^x$ and the photophysical properties of the lanthanide complexes together with the properties of the heterometallic $EuTbL^x_2$ (Scheme 1).

## EXPERIMENTAL SECTION

**General.** All chemicals were purchased from Acros and Sigma−Aldrich. Solvents were purchased from Sigma−Aldrich or Fisher. Deuterated solvents were purchased from Goss Scientific or Sigma−Aldrich and used as received. HPLC-grade solvents were used in photophysical studies. Water was deionized by use of an Elga Option 3 water purifier. All ligand and complex synthetic procedures were carried out under dinitrogen with degassed anhydrous solvents. $^1$H and $^{13}$C-{$^1$H} polarization enhancement nurtured during attached nucleus testing (PENDANT) NMR spectra were obtained on Brüker AC 300, AV 300, AMX 400, AV 400 or DRX 500 spectrometers. Electrospray mass spectra were recorded on a Micromass LC-TOF machine. Elemental analyses were recorded on a Carlo Erba EA1110 simultaneous CHN elemental analyzer at the University of Birmingham or by the CHN Microanalysis Service, School of Pharmacy, University of London.

**Photophysical Studies.** Steady-state luminescence experiments were carried out on a Photon Technology Instruments fluorescence system equipped a 75 W xenon arc lamp as the illumination source; single excitation and emission monochromators, the latter with grating blazed at 500 nm; a Hamamatsu R928 photomultiplier tube (PMT) for visible detection; and a Judson Technologies J 23 InGaAs photodiode cooled by thermoelectric cooling unit for near-infrared detection. The NIR signals were amplified by use of a Stanford Research Systems SR510 lock-in amplifier coupled to a PTI OC-4000 optical chopper. Spectra were recorded by use of PTI Felix fluorescence analysis software. The 77 K emission spectrum was recorded by use of a quartz electron paramagnetic resonance (EPR) tube fitted with a Young's tap. The peak with the asterisk in Figure 1 is attributed to scattering of the excitation light.

Quantum yields were measured by the optically dilute relative method[22] by use of the equation

$$\Phi_x = \Phi_r\left(\frac{A_r(\lambda_r)}{A_x(\lambda_x)}\right)\left(\frac{I_r(\lambda_r)}{I_x(\lambda_x)}\right)\left(\frac{n_x^2}{n_r^2}\right)\left(\frac{D_x}{D_r}\right)$$

where $\Phi_x$ is the quantum yield of the lanthanide complex, $\Phi_r$ is the quantum yield of reference, $A(\lambda)$ is the absorbance of a sample at excitation wavelength $\lambda$, $I(\lambda)$ is the relative intensity of excitation light at wavelength $\lambda$, $n$ is the refractive index of the solvent in question, and $D$ is the integrated area of the emission spectrum for sample and reference (corrected for PMT response). Ruthenium(II) tris(bipyridine) dichloride in aerated water[23] was used as standard for $Eu^{3+}$ and $Sm^{3+}$ quantum yield measurement. Quinine sulfate in aerated aqueous sulfuric acid

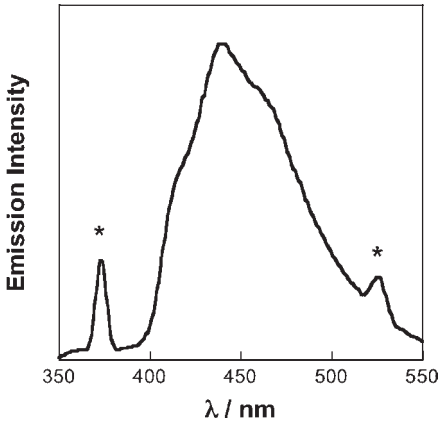


**Figure 1.** Emission spectrum of $GdL^x$ in methanol at 77 K, $\lambda_{exc}$ = 290 nm (*, scattering light).

(0.5 mol·dm$^{-3}$) was used as standard for $Tb^{3+}$ and $Dy^{3+}$ quantum yield measurements.[24]

Luminescence lifetimes in the visible were recorded by use of a Continuum Surelite I Nd:YAG laser (10 Hz) as the excitation source, with the 355 nm harmonic. Data were recorded on a LeCroy 9350AM 500 MHz oscilloscope as an average of 500 laser pulses, analyzed by use of Kaleidagraph software and fitted by a nonlinear least-squares iterative technique (Marquardt−Levenberg algorithm).[25]

UV−vis absorption spectra were recorded on a Shimadzu UV-3101PC UV−vis−NIR spectrometer.

**Diethylenetriamine-*N*,*N*′,*N*″-triacetic-*N*,*N*″-dianhydride [DTPA-bis(anhydride)].** By a modification to the reported procedure,[26] acetic anhydride (65.0 mL, 0.69 mol) was added dropwise to a stirring suspension of diethylenetriamine-*N*,*N*,*N*′,*N*″,*N*″-pentaacetic acid ($H_5$DTPA, 48.0 g, 0.12 mol) in anhydrous pyridine (50 mL) at 65 °C. Stirring was continued for a further 5 h while the temperature was maintained, after which time a light brown precipitate was collected by filtration. The precipitate was washed with acetic anhydride (200 mL) and brought to reflux in acetonitrile (250 mL) for 1 h. The resulting cream-colored precipitate was then isolated by filtration and washed with acetonitrile (2 × 50 mL) and diethyl ether (2 × 20 mL) to afford the title compound (37.7 g, 88%). All characterization data were in agreement with that previously reported by Wang et al.[27] $^1$H NMR (300 MHz, $D_2O$), $\delta$ ppm: 3.97 (8H, s, $NCH_2CO$), 3.62 (2H, s, $NCH_2CO_2H$), 3.46 (4H, t, $^3J$ = 6.2 Hz, $NCH_2CH_2N$), 3.16 (4H, t, $^3J$ = 6.2 Hz, $NCH_2CH_2N$). $^{13}$C{$^1$H} PENDANT NMR (75 MHz, $D_2O$), $\delta$ ppm: 173 ($CO_2H$), 170 (O—C═O), 120.9 ($NCH_2CO_2H$), 56.3 ($NCH_2COO$), 52.6 ($NCH_2CH_2N$), 49.9 ($NCH_2CH_2N$).

***N,N′*-Bis[*p*-thiophenyl(aminocarbonyl)]diethylenetriamine-*N,N′,N″*-triacetic Acid ($H_3L^x$).** 4-Aminothiophenol (2.00 g, 16.0 mmol) was added to a stirred suspension of DTPA-bis(anhydride) (1.02 g, 2.8 mmol) in anhydrous pyridine (10 mL). The mixture was stirred under nitrogen for 24 h at room temperature and the slightly cloudy yellow suspension was filtered. The volume of the solution was reduced *in vacuo* to give a thick yellow oil. Water (10 mL) was added to dissolve the oil, and the crude ligand was isolated by lowering the pH to 3 by dropwise addition of concentrated HCl. The aqueous layer was decanted and the isolated hygroscopic solid was washed with water (2 × 25 mL) and acetonitrile (2 × 25 mL) and then stirred in acetonitrile (2 × 50 mL) until a light yellow powder had formed. The powder was collected by suction filtration and washed with acetonitrile (2 × 10 mL) and diethyl ether (2 × 20 mL). Hydrazine monohydrate (3.0 mL, 3.1 g, 60.0 mmol) was then added dropwise to a solution of the crude product in pyridine (20 mL). The solvent was removed under vacuum, and the resulting oil was dissolved in water (10 mL) and filtered to yield a clear solution. The solution was acidified to pH 3 by dropwise addition of HCl. The white solid formed was isolated and washed with acetonitrile (2 × 25 mL) and then stirred in acetonitrile (2 × 50 mL) until a white powder had formed. The powder was collected by filtration and washed with acetonitrile (2 × 10 mL) and diethyl ether (2 × 20 mL) and then dried under vacuum to afford $\mathbf{H_3L^x}$ (0.67 g, 40%). $^1$H NMR (300 MHz, MeOH-$d_4$), $\delta$ ppm: 7.40 (4H, d, $^3J$ = 8.6 Hz, $H_f$); 7.13 (4H, d, $^3J$ = 8.6 Hz, $H_g$); 4.12 (2H, s, $H_a$); 3.62 (4H, s, $H_d$); 3.59 (4H, s, $H_e$); 3.49 (4H, t, $^3J$ = 5.2 Hz, $H_c$); 3.22 (4H, t, $^3J$ = 5.2 Hz, $H_b$). $^{13}$C {$^1$H} PENDANT NMR (75 MHz, MeOH-$d_4$), $\delta$ ppm: 172.8 ($\underline{C}O_2H$, $C_6$), 169.6 ($\underline{C}ONH$, $C_8$), 168.1 ($CO_2H$, $C_1$), 135.1 (Ar$\underline{C}$NHCO, $C_9$), 129.0 (Ar$\underline{C}$H, $C_{10}$), 126.0 (Ar$\underline{C}$SH, $C_{12}$), 120.5 (Ar$\underline{C}$H, $C_{11}$), 57.5 ($\underline{C}H_2$, $C_5$), 54.6 ($\underline{C}H_2$, $C_7$), 53.8 ($\underline{C}H_2$, $C_2$), 53.3 ($\underline{C}H_2$, $C_4$), 49.5 ($\underline{C}H_2$, $C_3$). MS (ES-TOF$^+$): $m/z$ 608 $\{M + H\}^+$, 630 $\{M + Na\}^+$. HRMS (ES-TOF) calcd for $C_{26}H_{32}N_5O_8S_2$: 606.1692. Found: 606.1697. Anal. Calcd for $C_{26}H_{33}N_5O_8S_2(N_2H_6Cl_2)_{0.6}(H_2O)_2$: C 44.2, H 5.8, N 12.3. Found: C 44.4, H 5.9, N 12.4. The large excess of hydrazine used in the reaction left some of dihydrochloride after acidic work-up. UV−vis (MeOH) $\lambda_{max}$, nm (log $\varepsilon$) 265 (4.5).

**Preparation of $LnL^x$ (where Ln = $La^{3+}$, $Nd^{3+}$, $Sm^{3+}$, $Eu^{3+}$, $Gd^{3+}$, $Dy^{3+}$, $Tb^{3+}$, $Er^{3+}$, and $Yb^{3+}$).** Two procedures, A and B, were followed. (A) $\mathbf{H_3L^x}$ (0.25 g, 0.40 mmol) was added to a solution of $LnCl_3 \cdot xH_2O$ (0.40 mmol) in degassed methanol (3 mL) and sonicated until all the ligand had dissolved. Acetonitrile (30 mL) was added to the solution yielding the complex as a white precipitate, which was collected by filtration under $N_2$, washed with acetonitrile and diethyl ether, and then dried in vacuo. (B) $\mathbf{H_3L^x}$ (0.20 g, 0.33 mmol) was dissolved in degassed methanol (5 mL). To the stirred solution was added KOH (0.055 g, 0.99 mmol) as a methanolic solution (5 mL), and the mixture was stirred for 10 min. The solvent was then removed under vacuum to yield the tripotassium salt $\mathbf{K_3L^x}$ in the reaction vessel, which was redissolved in degassed deionized water (5 mL). To the aqueous solution was added $LnCl_3 \cdot 6H_2O$ (1:1 $Ln^{3+}$:$\mathbf{K_3L^x}$, masses calculated as appropriate for each lanthanide salt). This caused an immediate precipitation of a white solid, which was isolated by suction filtration and washed with acetone (2 × 10 mL) and diethyl ether (5 mL) and then dried under vacuum to yield $\mathbf{LnL^x}$.

***LaL^x*.** Yield 83%. $^1$H NMR (300 MHz, MeOH-$d_4$), $\delta$ ppm: 7.60−7.10 (8H, Ar$\underline{H}$), 4.50−2.30 (18H, aliphatic $\underline{C}H_2$). $^{13}$C {$^1$H} PENDANT NMR (75 MHz, MeOH-$d_4$), $\delta$ ppm: 182.6−180.5 ($\underline{C}O_2H$, $\underline{C}ONH$), 136.2−134.3 (Ar$\underline{C}$), 130.5, 130.3 (Ar$\underline{C}$H), 128.6 (Ar$\underline{C}$), 124.1, 122.8, 122.0 (Ar$\underline{C}$H), 62.8−51.3 ($\underline{C}H_2$). MS (ES-TOF$^+$) $m/z$: 744 $\{M + H\}^+$, 766 $\{M + Na\}^+$. HRMS (ES-TOF) calcd for $LaC_{26}H_{31}N_5O_8S_2$: 744.0685. Found: 744.0678. UV−vis (MeOH) $\lambda_{max}$, nm (log $\varepsilon$): 266 (4.4).

***NdL^x*.** Yield 53−80%. MS (ES$^+$): $m/z$ 749 $[M + H]^+$, 771 $[M + Na]^+$. MS (ES-TOF$^+$): $m/z$ 789 $\{M + K\}^+$. HRMS (ES-TOF) calcd for $NdC_{26}H_{31}N_5O_8S_2$: 747.0691. Found: 747.0701. UV−vis (MeOH): $\lambda_{max}$, nm (log $\varepsilon$) 265 (4.4).

***SmL^x*.** Yield 81%. MS (ES-TOF$^+$) $m/z$: 756 $\{M + H\}^+$, 779 $\{M + Na\}^+$. HRMS (ES-TOF) calcd for $SmC_{26}H_{31}N_5O_8S_2$: 757.0811. Found: 757.0806. Anal. Calcd. for $SmC_{26}H_{31}N_5O_8S_2KCl(H_2O)$: C: 36.8, H 3.9, N 8.3. Found: C 36.8, H 4.3, N 8.2. UV−vis (MeOH) $\lambda_{max}$, nm (log $\varepsilon$): 266 (4.5).

***EuL^x*.** Yield 86%. MS (ES-TOF$^+$) $m/z$: 758 $\{M + H\}^+$, 794 $\{M + K\}^+$. HRMS (ES-TOF) calcd for $EuC_{26}H_{31}N_5O_8S_2$: 758.0826. Found: 758.0833. UV−vis (MeOH) $\lambda_{max}$, nm (log $\varepsilon$): 266 (4.4).

***GdL^x*.** Yield 71%. MS (ES-TOF$^+$) $m/z$: 763 $\{M+H\}^+$. HRMS (ES-TOF) calcd for $GdC_{26}H_{31}N_5O_8S_2$: 763.0855. Found: 763.0848. UV−vis (MeOH) $\lambda_{max}$, nm (log $\varepsilon$): 266 (4.3).

***TbL^x*.** Yield 86%. MS (ES-TOF$^+$) $m/z$: 764 $\{M + H\}^+$. HRMS (ES-TOF) calcd for $TbC_{26}H_{31}N_5O_8S_2$: 764.0868. Found: 764.0877. UV−vis (MeOH) $\lambda_{max}$, nm (log $\varepsilon$): 266 (4.6).

***DyL^x*.** Yield 65%. MS (ES-TOF$^+$) $m/z$: 767 $\{M + H\}^+$, 791 $\{M + Na\}^+$, 821 $\{M + K\}^+$. HRMS (ES-TOF) calcd for $DyC_{26}H_{31}N_5O_8S_2$: 769.0906. Found: 769.0921. UV−vis (MeOH) $\lambda_{max}$, nm (log $\varepsilon$): 266 (4.4).

***ErL^x*.** Yield 27%. MS (ES-TOF$^+$): $m/z$ 771 $\{M + Na\}^+$, 787 $\{M + K\}^+$. HRMS (ES-TOF) calcd for $NdC_{26}H_{31}N_5O_9S_2$: 771.0917. Found: 771.0913. UV−vis (MeOH): $\lambda_{max}$, nm (log $\varepsilon$) 265 (4.4).

***YbL^x*.** Yield 27%. MS (ES-TOF$^+$): $m/z$ 779 $\{M + H\}^+$, 802 $\{M + Na\}^+$, 817 $\{M + K\}^+$. HRMS (ES-TOF) calcd for $YbC_{26}H_{31}N_5O_8S_2$: 779.1003. Found: 779.0991. UV−vis (MeOH): $\lambda_{max}$, nm (log $\varepsilon$) 265 (4.4).

***N,N′*-Bis[*p*-(pyridyldithio)[phenyl(aminocarbonyl)]]diethylenetriamine-*N,N′,N″*-triacetic Acid ($H_3L^y$).** $\mathbf{H_3L^x}$ (0.30 g, 5.0 mmol) was dissolved in methanol (112 mL). The resulting solution was then added dropwise over a period of 20 min to a vigorously stirred solution of 2,2′-pyridyl disulfide (0.54 g, 25.0 mmol) in methanol (30 mL), and the mixture was stirred for a further 30 min, yielding a strongly colored yellow solution. The solvent was then removed under vacuum at 40 °C, giving a yellow oil that was redissolved in methanol (2 mL), and to which was added acetonitrile (50 mL) to precipitate crude $\mathbf{H_3L^y}$, which was stirred for 16 h at room temperature. The product was isolated by filtration and washed with acetonitrile (2 × 20 mL) and diethyl ether (10 mL) to yield $\mathbf{H_3L^y}$ as an initially hygroscopic cream-colored powder, which was dried under vacuum and stored under a nitrogen atmosphere (0.17 g, 42%). $^1$H NMR (300 MHz, MeOH-$d_4$), $\delta$ ppm: 8.41 (2H, m, $H_k$), 7.77 (4H, m, $H_{h,I}$), 7.44 (4H, d, $^3J$ = 8.8 Hz, $H_f$), 7.31 (4H, d, $^3J$ = 8.8 Hz, $H_g$), 7.14 (2H, m, $H_j$), 4.31 (2H, s, $H_a$), 3.64 (4H, s, $H_d$), 3.59 (4H, s, $H_e$), 3.52 (4H, t, $^3J$ = 5.1 Hz, $H_c$), 3.22 (4H, t, $^3J$ = 5.1 Hz, $H_b$). $^{13}$C {$^1$H} PENDANT NMR (75 MHz, MeOH-$d_4$), $\delta$ ppm: 175.2 ($\underline{C}OOH$, $C_6$), 172.5 ($\underline{C}ONH$, $C_5$), 170.3 ($\underline{C}OOH$, $C_1$), 161.6 ($\underline{C}$, $C_{13}$), 151.2 ($\underline{C}H$, $C_{17}$), 140.2 ($\underline{C}H$, $C_{15}$), 140.1 ($\underline{C}$, $C_9$), 133.0 ($\underline{C}$, $C_{12}$), 131.1 ($\underline{C}H$, $C_{10}$), 123.5 ($\underline{C}H$, $C_{14}$), 123.0 ($\underline{C}H$, $C_{11}$), 122.2 ($\underline{C}H$, $C_{16}$) 59.8 ($\underline{C}H_2$, $C_5$), 56.9 ($\underline{C}H_2$, $C_7$), 55.9 ($\underline{C}H_2$, $C_4$), 55.7 ($\underline{C}H_2$, $C_2$), 51.8 ($\underline{C}H_2$, $C_3$). MS (ES-TOF$^+$) $m/z$: 826 $\{M + H\}^+$, 848 $\{M + Na\}^+$. HRMS (ES-TOF) calcd for $C_{36}H_{39}N_7O_8S_4Na$: 848.1641. Found: 848.1657. Anal. Calcd for $C_{36}H_{39}N_7O_8S_4(N_2H_6Cl_2)_{0.25}(H_2O)_{0.6}$: C 50.1, H 4.9, N 12.2. Found: C 49.8, H 5.0, N 11.9. UV−vis (MeOH) $\lambda_{max}$, nm (log $\varepsilon$): 262 (4.5), 285(sh) (4.4).

## RESULTS AND DISCUSSION

**Synthesis and Characterization of $H_3L^x$ and $H_3L^y$.** $\mathbf{H_3L^x}$ was prepared from the reaction of 4-aminothiophenol with DTPA-bis(anhydride) in anhydrous pyridine (Scheme 2). The dual acylation proceeded smoothly to form the desired product in respectable yield and high purity. Hydrazine monohydrate was used midsynthesis to reduce any disulfides in the crude product to thiols, under mild conditions.

The 300 MHz $^1$H NMR spectrum of $\mathbf{H_3L^x}$ in methanol-$d_4$ shows resonances in the aromatic and aliphatic regions of the

**Scheme 2. Synthetic Route for $H_3L^x$ and $H_3L^y$**

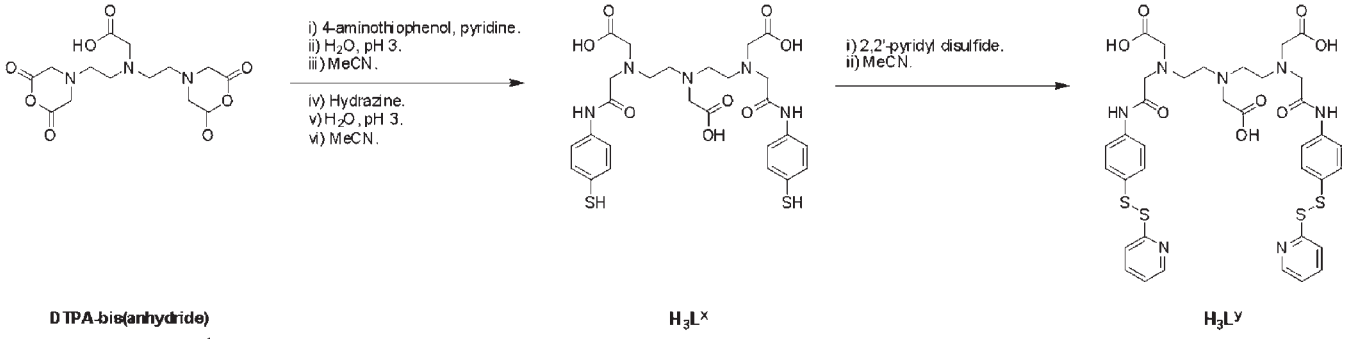


spectrum (Supporting Information). Although there are several reports of NMR spectra of DTPA-bis(amide) derivatives,[27−34,42,35] few of them have observed the detailed features. Our results agree with the characteristic backbone features for substituted DTPA-bis(amides). The aromatic protons $H_f$ and $H_g$ appear at 7.40 and 7.13 ppm, respectively, as 4H doublets (AB system). In the aliphatic region the central $CH_2$ protons $H_a$ appear as a unique 2H singlet at 4.12 ppm. The protons $H_d$ and $H_e$, which correspond to the amide and terminal carboxylic acid "arms", appear as two separate 4H singlets, with the carboxylic acid appended $H_d$ appearing slightly further downfield at 3.62 ppm compared to the amide-bound $H_e$, which appear at 3.59 ppm due to the slightly more electron-withdrawing carboxylic acid group compared to the amide. The ethylenic backbone protons $H_b$ and $H_c$ appear at 3.49 and 3.22 ppm, respectively, manifesting themselves as two separate 4H triplets. The 75 MHz $^{13}C\{^1H\}$ PENDANT NMR spectrum of $\mathbf{H_3L^x}$ in methanol-$d_4$ shows 12 carbon resonances at the expected chemical shifts. The aromatic region from 110 to 150 ppm displays four signals, two C−H and two quaternary carbon resonances, consistent with the thiophenol ring systems appended (Supporting Information). The UV−vis absorption spectrum of $\mathbf{H_3L^x}$ in methanol (Supporting Information) shows a single $\pi-\pi^*$ band with $\lambda_{max}$ = 265 nm and a molar absorptivity coefficient of log $\varepsilon$ = 4.5.

$\mathbf{H_3L^y}$ was synthesized by reaction of $\mathbf{H_3L^x}$ with 5 equiv of 2,2′-pyridyl disulfide (Scheme 1). Reaction was evidenced by the appearance of a strong yellow color corresponding to the liberation of the chromophore. The reaction was run at a relatively low concentration with good mixing to avoid generation of symmetric $\mathbf{H_6L_2^x}$ and polymeric species (by competing thiol−disulfide exchange). NMR spectroscopy was used to monitor the transformation of $\mathbf{H_3L^x}$ to $\mathbf{H_3L^y}$. The $^1H$ NMR spectrum (Supporting Information) gave evidence of reaction by the appearance of pyridyl ring resonances in the aromatic region at 8.41, 7.77, and 7.14 ppm, integrating exactly for 2H, 4H, and 2H. We have assigned these resonances as $H_k$, $H_h/H_i$, and $H_j$, respectively, on the basis of previously reported pyridyl sulfide chemical shifts.[36,37] The formation of the two disulfide bonds is evidenced by the shift of the proton $H_g$ from 7.13 ppm in $\mathbf{H_3L^x}$ to 7.31 ppm in $\mathbf{H_3L^y}$. The 75 MHz $^{13}C\{^1H\}$ PENDANT NMR spectrum of $\mathbf{H_3L^y}$ (Supporting Information) gave further verification of ligand formation with the appearance of resonances corresponding to $C_{13}$, $C_{17}$, $C_{15}$, $C_{14}$, and $C_{16}$ at 161.6, 151.2, 140.2, 123.5, and 122.6 ppm, respectively. The latter assignments were made by correlation with the $^{13}C\{^1H\}$ PENDANT NMR spectrum of the 2,2′-pyridyl disulfide starting material. Positive-mode electrospray mass spectrometry identified $\mathbf{H_3L^y}$ as the sole species, showing $\{M + H\}^+$ and $\{M + Na\}^+$ peaks at $m/z$ 826 and 843 respectively with high-resolution spectra confirming the mass of the ligand to be within 2 ppm of the calculated value. The UV−vis absorption spectrum of $\mathbf{H_3L^y}$ (Supporting Information) gives further evidence to the aromatic modification with a new shoulder appearing at 285 nm, which is attributed to the $\pi-\pi^*$ absorption of the pyridyl group,[38] superimposed upon the original $\pi-\pi^*$ absorption of the amidophenyl group.

**Scheme 3. Chemical Structure of $\mathbf{LnL^x}$**

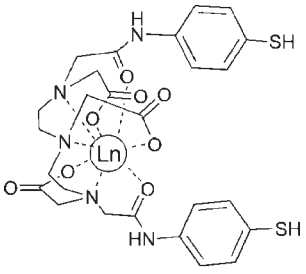


$\mathbf{LnL^x}$

**Synthesis and Characterization of $\mathbf{LnL^x}$ (where Ln = $La^{3+}$, $Nd^{3+}$, $Sm^{3+}$, $Eu^{3+}$, $Gd^{3+}$, $Dy^{3+}$, $Tb^{3+}$, $Er^{3+}$, and $Yb^{3+}$).** The lanthanide(III) complexes of $\mathbf{H_3L^x}$ (Scheme 3) were synthesized either via preparation of the tripotassium salt $\mathbf{K_3L^x}$ or via direct reaction and isolation with the corresponding lanthanide chloride.

Positive-mode electrospray ionization time-of-flight mass spectrometry (ES-TOF) was used to identify $\mathbf{LnL^x}$. Mass spectra of the lanthanide complexes showed the correct $\{M + H\}^+$ peak in all cases, with small amounts of either the sodium or potassium adducts, which is a result of the ionization conditions. The characteristic isotope patterns of the complex peaks in the mass spectra can be used as a signature of the incorporation of $Ln^{3+}$; all complexes displayed the correct isotope patterns. Electrospray ionization high-resolution mass spectrometry was used to obtain the exact monoisotopic masses of $\mathbf{LnL^x}$. The high-resolution mass of the complexes matched the theoretical mass within ±5 ppm in all cases.

As a result of its diamagnetic nature, it was possible to further study $\mathbf{LaL^x}$ by NMR spectroscopy. The 300 MHz $^1H$ NMR spectrum of $\mathbf{LaL^x}$ in methanol-$d_4$ displays two distinct areas of resonances (Supporting Information). The aromatic region of the spectrum shows manifold peaks ranging from 7.60 to 7.10 ppm. This manifold corresponds to the aromatic CH protons on the amidothiophenol ring system and integrates for eight protons. The aliphatic region displays the same pseudomultiplet


dx.doi.org/10.1021/ja109157g |J. Am. Chem. Soc. 2011, 133, 1033–1043

appearance with broad resonances ranging from 4.50 to 2.30 ppm; these correspond to the aliphatic $CH_2$ protons on the DTPA backbone and integrate for 18H in total if integration of the methanol solvent signal is subtracted. The resonances are broadened[33,35,39] by the presence of rapidly interchanging rotamers of the ligand backbone surrounding the lanthanide metal center in solution. In the 75 MHz $^{13}C\{^1H\}$ PENDANT NMR spectrum of **LaL$^x$** (Supporting Information), resonances are observed in the expected regions: carboxylic acid and amide resonances between 190 and 160 ppm, aromatic resonances between 140 and 110 ppm, and aliphatic resonances between 70 and 45 ppm.

We used the **GdL$^x$** complex to probe the triplet energy level of the aromatic thiophenyl sensitizer to assess its efficiency in the energy-transfer process to the lanthanides. Gadolinium(III) complexes are a popular choice for elucidating ligand triplet energy levels, and the reasons for this are two-fold: (i) The heavy $Gd^{3+}$ ion increases the rate of intersystem crossing from singlet to triplet (the so-called "internal heavy atom effect") in the ligand, and (ii) $Gd^{3+}$ has no accessible energy levels into which the ligand can subsequently transfer energy. Hence, radiative decay from an excited triplet state becomes the predominant photophysical pathway. **GdL$^x$** exhibits ligand phosphorescence as a broad band centered at 440 nm after excitation at 290 nm in degassed methanol at 77 K (Figure 1). The spectrum clearly shows the vibrational structure of the phosphorescence centered at 440 nm.

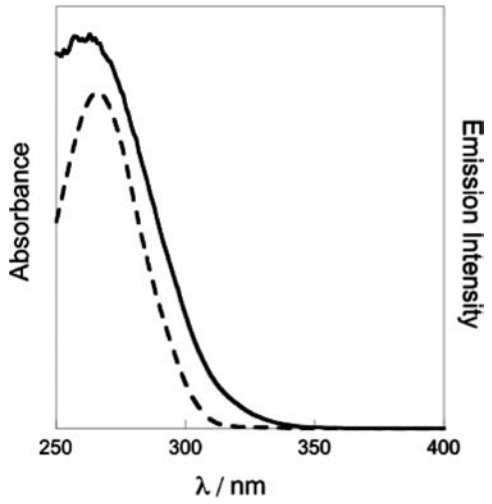


**Figure 2.** Absorption (dashed line) and excitation spectra with $\lambda_{em}$ = 545 nm (solid line) of **TbL$^x$**. The excitation spectrum is corrected for lamp response.

The triplet-state energy level was calculated to be 24 100 $cm^{-1}$ from the (0−0) transition, comparable with the triplet energy levels observed for benzene (29 500 $cm^{-1}$) and aminobenzene (24 800 $cm^{-1}$) in polar solvents.[40] Calculation of the triplet energy of **GdL$^x$** shows that the level is well-positioned for energy transfer into a range of visible-emitting lanthanide luminescent states,[41,42] including those of $Eu^{3+}$ ($^5D_0$, 17 300 $cm^{-1}$), $Sm^{3+}$ ($^4G_{5/2}$, 17 900 $cm^{-1}$), $Tb^{3+}$($^5D_4$, 20 500 $cm^{-1}$), and $Dy^{3+}$ ($^4F_{9/2}$, 21 100 $cm^{-1}$), and yet acting as donor for the NIR-emitting states of $Nd^{3+}$ (11 200 $cm^{-1}$), $Yb^{3+}$ (10 300 $cm^{-1}$), and $Er^{3+}$ (6500 $cm^{-1}$). The excitation spectrum of **TbL$^x$** monitored at the strongest f−f transition at 545 nm ($^5D_4 \rightarrow {}^7F_5$) shows a broad band with $\lambda_{max}$ at 266 nm (Figure 2). This closely resembles the profile of the absorption spectrum, which demonstrates that an energy transfer from the two phenyl groups sensitizes the lanthanide luminescence exhibited by **TbL$^x$**. Similar excitation profiles are observed by monitoring emission of **EuL$^x$** at 614 nm ($^5D_0 \rightarrow {}^7F_2$), **SmL$^x$** at 596 nm ($^4G_{5/2} \rightarrow {}^6H_{7/2}$), and **DyL$^x$** at 484 nm ($^4F_{9/2} \rightarrow {}^6H_{15/2}$).

The emission spectra of all four visible emitting complexes show typical narrow-band lanthanide luminescence after excitation into the ligand-based phenyl $\pi-\pi^*$ absorption band at 266 nm (Figure 3). Irradiation of **SmL$^x$** with UV light at 266 nm leads to pink emission assigned to the $^4G_{5/2} \rightarrow {}^6H_J$ transitions of $Sm^{3+}$ (where $J$ = $^5/_2$, $^7/_2$, and $^9/_2$). **EuL$^x$**, **TbL$^x$**, and **DyL$^x$** are also emissive, with the characteristic bands observed for each complex after excitation at 266 nm. **EuL$^x$** displays red emission that is

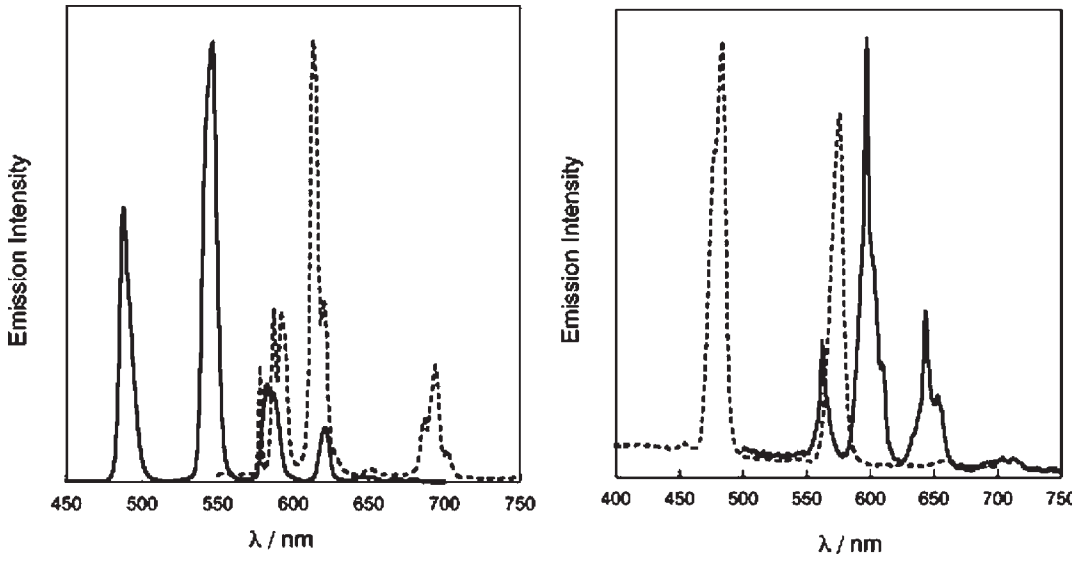


**Figure 3.** Normalized emission spectra of (a) **TbL$^x$** (solid line) and **EuL$^x$** (dashed line) in methanol, $\lambda_{exc}$ = 266 nm, and (b) **SmL$^x$** (solid line) and **DyL$^x$** (dashed line) in methanol, $\lambda_{exc}$ = 266 nm.


dx.doi.org/10.1021/ja109157g |*J. Am. Chem. Soc.* 2011, 133, 1033–1043

**Table 1. Luminescence Lifetimes and Number of Inner-Sphere Methanol Molecules for $LnL^x$**

| $LnL^x$ | $\tau_{MeOH}$(ms) | $\tau_{MeOD}$(ms) | $m$ |
|---|---|---|---|
| $EuL^x$ | 0.84 | 1.75 | $1.3 \pm 0.5$ |
| $TbL^x$ | 1.43 | 1.98 | $1.6 \pm 0.5$ |
| $SmL^x$ | 0.014 | 0.025 | $1.5 \pm 0.5$ |
| $DyL^x$ | 0.018 | 0.024 | |

assigned to the $^5D_0 \rightarrow {}^7F_J$ transitions of $Eu^{3+}$ ($J$ = 0, 1, 2, 3, and 4) at $\lambda$ = 578, 590, 613, 650, and 695 nm, respectively. Excitation of $\mathbf{TbL^x}$ at 266 nm leads to green emission from the $^5D_4 \rightarrow {}^7F_J$ transitions of $Tb^{3+}$ ($J$ = 6, 5, 4, 3, 2, 1, and 0) at $\lambda$ = 487, 545, 585, 621, 650, 668, and 680 nm, respectively. Similarly, through-ligand sensitization of $\mathbf{DyL^x}$ leads to typical yellow $Dy^{3+}$ emission from the $^4F_{9/2} \rightarrow {}^6H_J$ transitions ($J = {}^{15}/_2$, ${}^{13}/_2$, and ${}^{11}/_2$) at $\lambda$ = 484, 577, and 660 nm, respectively.

The spectra of the isolated complexes agree with those obtained when the complexes were formed *in situ* with addition of equimolar solution of the lanthanide chloride into solution of $\mathbf{H_3L^x}$. The solutions formed in situ showed the characteristic complex peaks in the electrospray mass spectra, in agreement with the isolated complexes.

The rate of decay of each luminescent state was measured by time-resolved luminescence spectroscopy and the lifetimes are reported in Table 1. In all cases, the measurement of luminescence lifetimes led to monoexponential fittings of the decay curve, indicating the presence of a single lanthanide coordination environment.

Calculation of the number of inner-sphere methanol molecules,[43] $m$, by use of eq 1 led to an average of $1.5 \pm 0.5$ per $\mathbf{LnL^x}$:

$$m = A(k_{MeOH} - k_{MeOD}) \quad (1)$$

where $A$ is an experimentally determined lanthanide-specific quenching constant that reflects the susceptibility to radiationless vibrational decay from hydroxyl oscillators for a certain lanthanide ion ($A$ = 8.4, 2.1, and 0.05 ms for $Tb^{3+}$, $Eu^{3+}$, and $Sm^{3+}$)[43,44] and $k$ is the rate of luminescence decay (reciprocal luminescence lifetime), per millisecond, in deuterated and non-deuterated solvents. The noninteger values obtained for $\mathbf{LnL^x}$ reflect both the quenching contribution of outer-sphere solvent molecules and the possibility of some molecules bearing one or two coordinated solvent molecules. The reported crystal structures of the ethyl-[34] and benzyl-[32] substituted DTPA-bis(amide) complexes show one solvent molecule to be bound on the lanthanide center. The lower values of the luminescence lifetimes for $\mathbf{SmL^x}$ and $\mathbf{DyL^x}$ are attributed to the additional deactivation pathways of their excited states. The vibrational deactivation of the luminescent state by hydroxyl and amide oscillators ($\nu_{OH}$ = 3300−3500 $cm^{-1}$, $\nu_{NH}$ = 3100−3300 $cm^{-1}$) is particularly efficient due to the small energy gap between the luminescent-state and ground-state manifolds: those lanthanides with smaller energy gaps (e.g., $Dy^{3+}$ and $Sm^{3+}$) are quenched more efficiently than for lanthanides with larger energy gaps (e.g., $Eu^{3+}$ and $Tb^{3+}$) due to better vibronic coupling as dictated by the energy gap law and Franck−Condon factors.[45] The shorter lifetime of $\mathbf{EuL^x}$ compared to $\mathbf{TbL^x}$ is attributed to the presence of an ligand to metal charge transfer (LMCT) state in the easily reduced europium complex ($E^0$ = −0.35 V) from the carboxylate ligands that quench the europium excited state.[46,47]

The luminescence quantum yields of $\mathbf{TbL^x}$ and $\mathbf{EuL^x}$ in methanol were found to be 0.32% and 0.04%, respectively. The values take into account the efficiency of the overall energy-transfer process from the phenyl sensitizer to the lanthanide ion, affected by the rather high level of the triplet state of the sensitizer (24 100 $cm^{-1}$), responsible for the energy transfer, in comparison with the lanthanide excited state; the sensitizer's distance from the luminescent center; and the presence of other deactivation processes originating from charge-transfer states or other nonradiative states and vibronic coupling. Clearly, the phenyl sensitizer may not an have ideally matched triplet state with the lanthanide, and also the heavy atom effect may not be as efficient in promoting the population of the triplet state due to the distance between the lanthanide center and the sensitizer. For $\mathbf{DyL^x}$ and $\mathbf{SmL^x}$, the quantum yields were measured to be 0.03% and 0.02%, respectively; the low values are not surprising since their luminescence signal is affected by additional quenching mechanisms as aforementioned in the discussion of the lifetimes.[48]

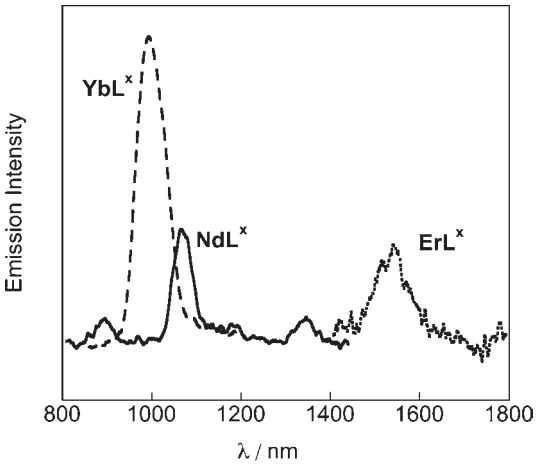


**Figure 4.** Emission spectra of $\mathbf{NdL^x}$ (solid line), $\mathbf{YbL^x}$ (dashed line), and $\mathbf{ErL^x}$ (dotted line) in methanol-$d_1$, $\lambda_{exc}$ = 265 nm.

The triplet state of the 4-amidothiophenol sensitizer also proved suitable for sensitization of a range of NIR-emitting lanthanide ions. Luminescence spectra of $\mathbf{NdL^x}$, $\mathbf{ErL^x}$, and $\mathbf{YbL^x}$ after excitation into the thiophenol $\pi-\pi^*$ transition displayed typical narrow-band emission in the NIR region (Figure 4). Irradiation of $\mathbf{NdL^x}$ at 265 nm leads to characteristic emission bands at 890, 1064, and 1340 nm, which correspond to the $^4F_{3/2} \rightarrow {}^4I_J$ ($J = {}^9/_2$, ${}^{11}/_2$, and ${}^{13}/_2$) f−f transitions of the $Nd^{3+}$ ion. Similarly, excitation of $\mathbf{YbL^x}$ at 265 nm leads to a single emission band at 993 nm, corresponding to the $^2F_{5/2} \rightarrow {}^2F_{7/2}$ transition of the $Yb^{3+}$ ion. Excitation of $\mathbf{ErL^x}$ at 265 nm also leads to NIR emission, with a single band centered at 1535 nm, assigned to the $^4I_{13/2} \rightarrow {}^4I_{15/2}$ transition of the $Er^{3+}$ ion. These steady-state luminescence experiments were performed in deuterated methanol-$d_1$ to avoid quenching by hydroxyl oscillators.[48,49]

To confirm that the transfer of energy from the thiophenol antenna chromophore to the lanthanide ion was responsible for the luminescence observed, excitation spectra were recorded for all the NIR-emitting complexes. Monitoring of $\mathbf{YbL^x}$, $\mathbf{NdL^x}$, and $\mathbf{ErL^x}$ at their strongest emission bands (980, 1060, and 1530 nm, respectively) led to excitation spectra with profiles similar to those of the UV−vis absorption spectra (Supporting Information). It is worthwhile noting that, in contrast to the excitation spectra recorded for the visible-emitting complexes, the bathochromic wavelengths of the $\pi-\pi^*$ absorption band are relatively more effective in sensitizing the emission from the lanthanide ion, and as a result the excitation band is much broader in

**Scheme 4. Heterometallic Macrocycle Assembly in Solution by Use of Activated Thiols**

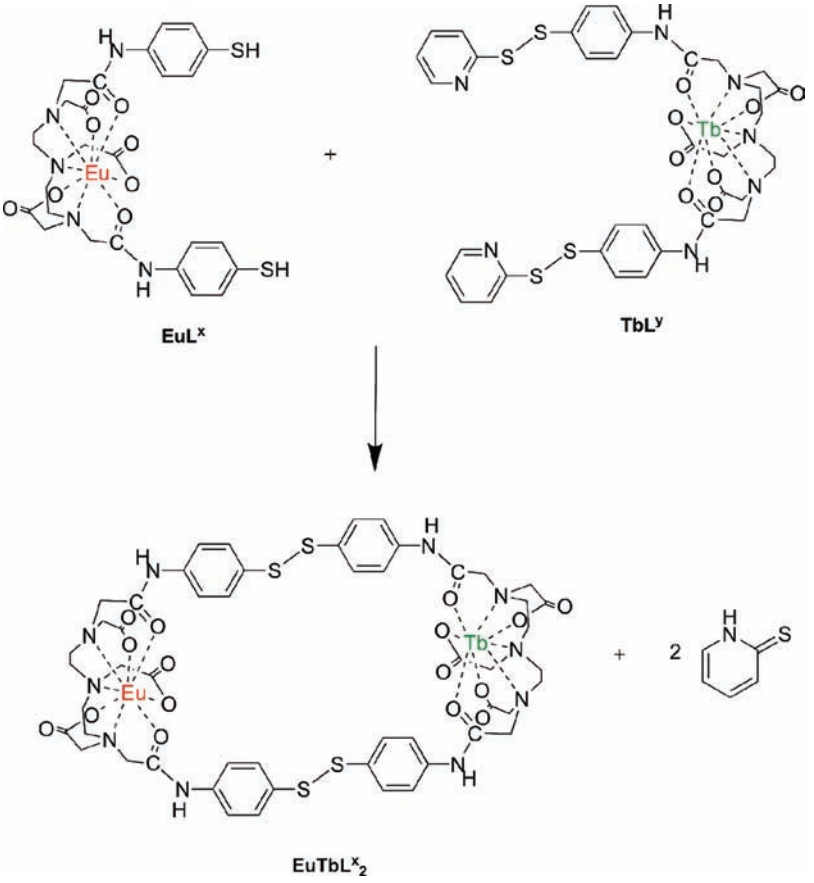


the cases of the NIR-emitting complexes than for the visible complexes.

**Controlled Assembly of Heterometallic $LnLn'L^x_2$ Dimers.** We introduce an activated thiol in the thiol−disulfide exchange chemistry for the solution assembly of $\mathbf{LnLn'L^x_2}$ macrocycles (Scheme 4). Converse to the usual reversible mechanism of thiol−disulfide exchange, observed in such biological processes as protein folding and recently exploited in dynamic combinatorial libraries,[50−52] the activation reaction does not favor the reverse reaction.[53] This is due to the dominance of the 2-pyridylthione tautomer at room temperature,[52] which cannot be fed back in to the reverse pathway as a thiol would. The release of the 2-pyridylthione chromophore leads to a rise in absorption at 353 nm in methanol. Utilizing this chemistry we were able to assemble europium−terbium macrocycles in solution, monitoring the controlled assembly by UV−vis spectroscopy, and using electrospray mass spectrometry and luminescence spectroscopy for their full solution characterization.

Heterometallic $\mathbf{EuTbL^x_2}$ macrocycles (Scheme 4) were formed in methanolic solution by reaction of a solution of $\mathbf{EuL^x}$ (25 $\mu$mol·dm$^{-3}$) and an equimolar solution of the activated $\mathbf{TbL^y}$. The reaction was monitored by UV−vis absorption spectroscopy at time intervals of 0, 5, 10, 15, 20, 25, and 30 min (Figure 5). The appearance of the 353 nm peak is characteristic of the presence of the pyridyl-2-thione chromophore. A plot of the increasing absorbance values at 353 nm versus time shows a sharp increase followed by a shallow curve profile, which plateaus when absorbance reaches about 0.15, demonstrating the

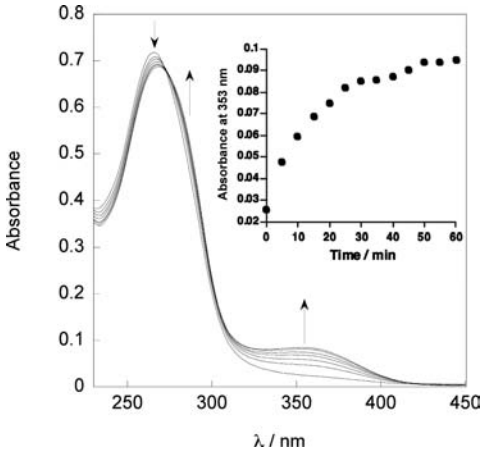


**Figure 5.** UV−vis absorption spectra of the solution containing $\mathbf{EuL^x}$ (25 $\mu$mol·dm$^{-3}$) with $\mathbf{TbL^y}$ (25 $\mu$mol·dm$^{-3}$) at time intervals of 0, 5, 10, 15, 20, 25, and 30 min, where 0 min is the mixing of the two solutions. Inset: Plot of absorbance at 353 nm vs time for the same experiment.

release of the pyridyl-2-thione and the binding event of $\mathbf{EuL^x}$ and $\mathbf{TbL^y}$ (Figure 5, inset). This two-step profile agrees with a fast initial binding followed by a slow reorganization step of macrocycle closure. Furthermore, the binding of the two lanthanide complexes is confirmed by the observation of the isosbestic points.

The final absorbance of the solution at 353 nm is in agreement with the release of 25 $\mu$mol·dm$^{-3}$ solution of 2-pyridylthione as


dx.doi.org/10.1021/ja109157g |J. Am. Chem. Soc. 2011, 133, 1033–1043

calculated by its molar absorptivity, $\varepsilon$, at 353 nm (Supporting Information). In this case the binding is clearly weaker and the curve does not show the two-step profile. As a control experiment, we also examined the reactivity of a solution of 25 $\mu$mol·dm$^{-3}$ $\mathbf{H_3L^y}$ with 6 equiv of 4-acetamidothiophenol, which led to the displacement of 2-pyridylthione with the expected final absorbance at 353 nm of around $A$ = 0.3 (Supporting Information). It is worth noting that the binding in this case is weaker and does not show the two-step effect.

The final absorbance of the solution at 353 nm is in agreement with the release of 25 $\mu$mol·dm$^{-3}$ solution of 2-pyridylthione as calculated by its molar absorptivity, $\varepsilon$, at 353 nm (Supporting Information). In this case the binding is clearly weaker and the curve does not show the two-step profile. As a control experiment we also examined the reactivity of a solution of 25 $\mu$mol·dm$^{-3}$ $\mathbf{H_3L^y}$ with 6 equiv of 4-acetamidothiophenol which led to the displacement of 2-pyridylthione with the expected final absorbance at 353 nm of around $A$ = 0.3 (Supporting Information). It is worth noting that the binding in this case is weaker and does not show the two-step effect.

Positive-mode electrospray mass spectrometry was used to examine the formation of heterometallic macrocycles in solution (Figure 6). The *controlled* assembly of $\mathbf{EuTbL^x_2}$, by our approach as indicated in Scheme 4, gave a single peak manifold centered at $m/z$ 781 corresponding to the doubly charged $\{M + H + Na\}^{2+}$ heterometallic $\mathbf{EuTbL^x_2}$ macrocycle (Figure 6a). No homometallic species were observed in this mass spectrum. We examined the statistical assembly of the species $\mathbf{EuTbL^x_2}$ to contrast with the controlled formation of the $\mathbf{EuTbL^x_2}$ by reacting $\mathbf{EuL^x}$ and $\mathbf{TbL^x}$ (25 $\mu$mol·dm$^{-3}$) under mild dimethyl sulfoxide co-oxidation conditions (20% DMSO in methanol or *N*,*N*-dimethylformamide, DMF) (Scheme 5).[54] The mass spectral analysis of this solution indicated the presence of all three possible $\mathbf{Eu_2L^x_2}$, $\mathbf{EuTbL^x_2}$, and $\mathbf{Tb_2L^x_2}$ macrocyclic species with peak manifolds of the doubly charged $\{M + 2H\}^{2+}$ ions at $m/z$ 756, 759, and 762, respectively (Figure 6b). The individual isotope patterns serve to act as a signature of double lanthanide incorporation in the macrocycles.

Solutions of $\mathbf{EuTbL^x_2}$ show typical narrow-band lanthanide luminescence upon excitation at 266 nm (Figure 7). Emission bands originating from both the europium and terbium centers are observed as expected for a complex incorporating both metal centers. This leads to an interesting emission spectrum ranging from 450 to 750 nm, which is attractive with respect to the optoelectronic ability of the complex to be tuned to a desired emission wavelength for certain applications in luminescent sensing or in optical devices.

In order to examine whether there is communication between $Tb^{3+}$ and $Eu^{3+}$ centers in the form of photoinduced energy transfer (the $^5D_4$ state of $Tb^{3+}$ lies 3200 cm$^{-1}$ higher than the

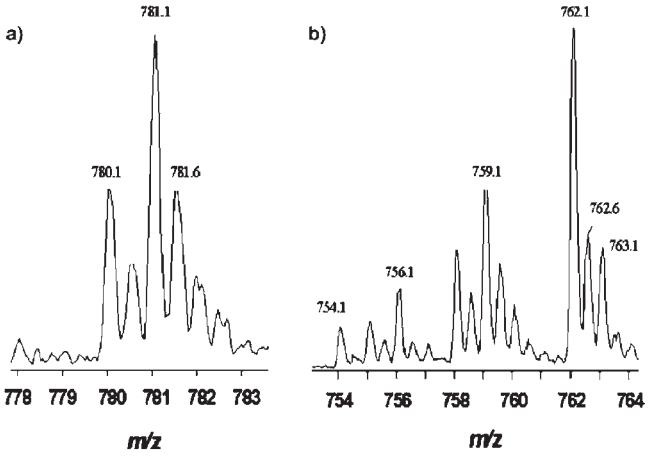


**Figure 6.** ES-MS$^+$ of macrocyclic lanthanide species prepared by (a) controlled assembly of $\mathbf{EuTbL^x_2}$ with the activated thiol approach or (b) statistical assembly under mild oxidative conditions, leading to peaks for $\mathbf{Eu_2L^x_2}$, $\mathbf{EuTbL^x_2}$, and $\mathbf{Tb_2L^x_2}$.

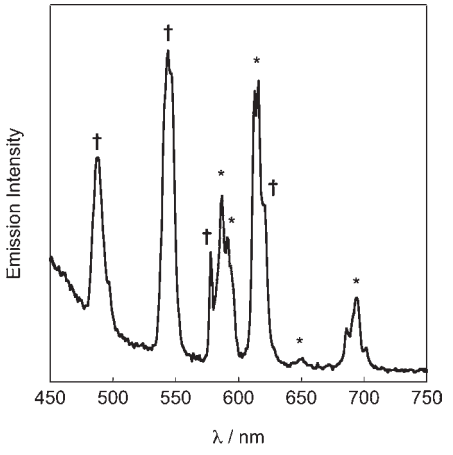


**Figure 7.** Emission spectrum of $\mathbf{EuTbL^x_2}$ in methanol, $\lambda_{exc}$ = 266 nm. Bands arising from $Tb^{3+}$ emission assigned to $^5D_4 \rightarrow {}^7F_J$ ($J$ = 6−3) are indicated by daggers (†). Bands arising from $Eu^{3+}$ emission assigned to $^5D_0 \rightarrow {}^7F_J$ ($J$ = 0−4) are indicated by asterisks (*).

**Scheme 5. Activated Thiol Assembly versus Statistical Assembly for Heterometallic Lanthanide Complexes**

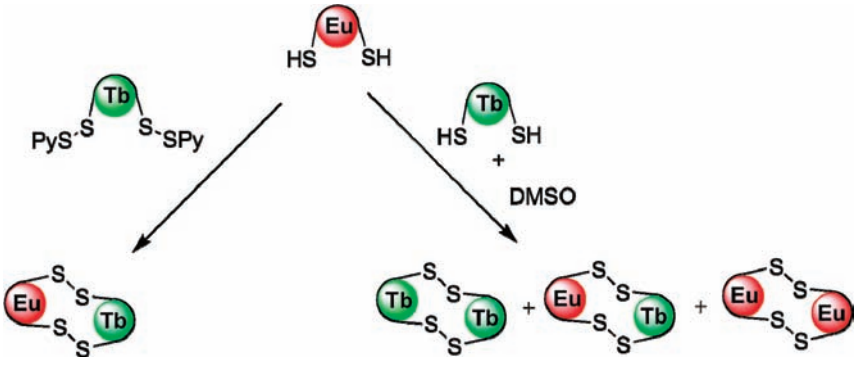



dx.doi.org/10.1021/ja109157g |*J. Am. Chem. Soc.* 2011, 133, 1033–1043

$^5D_0$ of $Eu^{3+}$), we used time-resolved luminescence spectroscopy by monitoring the $^5D_4 \rightarrow {}^7F_6$ emission band of the $Tb^{3+}$ ion as a potential energy donor (Scheme 6). The energy transfer steps ET1 and ET2 (Scheme 6) are the ones taking place from the phenyl chromophore to the lanthanide and the processes are known to occur on the picosecond time scale;[55] hence they are not anticipated to affect the intralanthanide energy transfer step ET3. The luminescence lifetime of a methanolic solution of $\mathbf{EuTbL^x_2}$ was found to be 0.5 ms, reduced by two-thirds in comparison with 1.5 ms in homometallic $\mathbf{Tb_2L^x_2}$. This deactivation of the luminescent $^5D_4$ state in $Tb^{3+}$ can only be attributed to a photoinduced process taking place between terbium and europium ions. The luminescence signal of $\mathbf{EuL^x}$ was monitored at the position of the $^5D_4 \rightarrow {}^7F_6$ transition of $Tb^{3+}$ under time-resolved conditions as a control experiment. As expected, no emission signal was detected at this wavelength, which showed that the shortened lifetime in $\mathbf{EuTbL^x_2}$ at 487 nm has no contribution from direct $Eu^{3+}$ luminescence and must be caused purely by a reduction of $Tb^{3+}$ luminescent lifetime. Although electron transfer may also be a possibility between metal centers, previous studies on energy transfer between pairs of $Eu^{3+}$ and $Tb^{3+}$ ions in free solution,[56] as well as those encapsulated in ligand frameworks[57,58] and protein scaffolds,[59] tend to agree that energy transfer from $Tb^{3+}$ to $Eu^{3+}$ proceeds through nonradiative mechanisms and it is the most favorable step; indeed, energy transfer between lanthanide centers is commonly attributed to a dipole−dipole interaction, which is anticipated in fundamental terms due to the buried nature of the f orbitals in the lanthanide ions.

The energy-transfer efficiency ($\eta$) for the purely dipole−dipole, through-space energy-transfer mechanism can be quantified[58] by eqs 2 and 3:

$$\eta = 1/[1 + (R/R_0)^6] \quad (2)$$

$$\eta = 1 - (\tau/\tau_0) \quad (3)$$

**Scheme 6. Simplified Energy Diagram of Relevant Energy Levels That Participate in the Energy Transfer from $Tb^{3+}$ to $Eu^{3+}$**

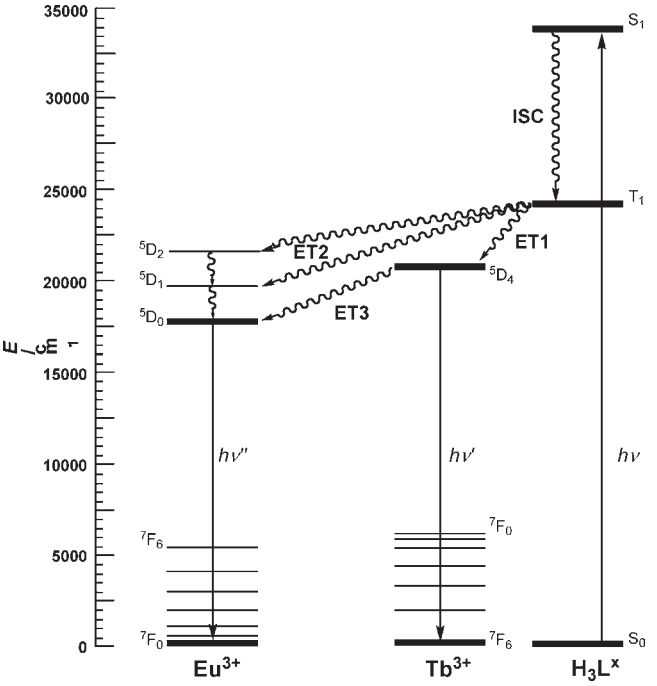


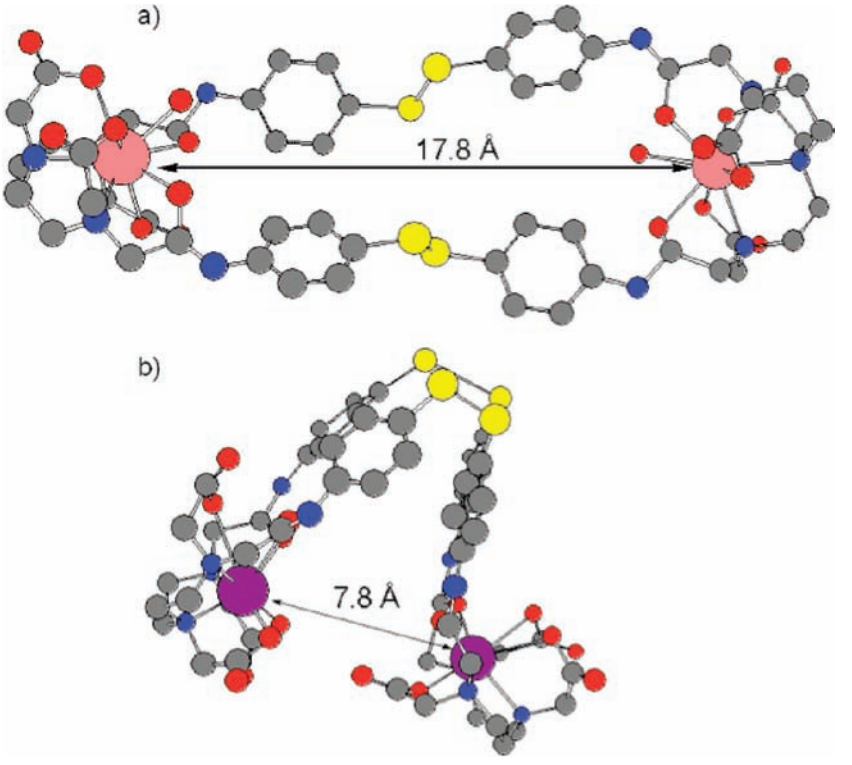


**Figure 8.** Models of $\mathbf{EuTbL^x_2}$ macrocycle: (a) in protracted pseudo-*exo* state with *trans*-disulfides and (b) in pseudo-*endo* state with *cis*-disulfide bridges. Distances between lanthanide centers are given in angstroms.


dx.doi.org/10.1021/ja109157g | *J. Am. Chem. Soc.* 2011, 133, 1033–1043

where $R_0$ is the distance required for 50% energy transfer, $R$ is the actual distance between donor and acceptor, and $\tau$ and $\tau_0$ are the lifetimes of luminescence of the donor in the presence and absence of acceptor. The value for $R_0$ usually lies between 8 and 10 Å for $Eu^{3+}$—$Tb^{3+}$ pairs in helicates[58] and is quoted as 8.31 Å for the free ions in dimethyl sulfoxide solution.[56] An MM2 energy minimization[60] of a model of $\mathbf{EuTbL^x_2}$ led to a protracted complex with an interlanthanide distance of 17.8 Å (Figure 8a). Using this value of 17.8 Å for $R$ and an average value of 9.0 Å for $R_0$ with eq 2, we obtain a theoretical energy-transfer efficiency of $\eta$ = 1.6%. However, use of eq 3 shows that from the lifetime measurements we experimentally estimate an energy-transfer efficiency of $\eta$ = 66% when $\tau$ = 0.5 ms and $\tau_0$ = 1.5 ms. The observed efficiency of energy transfer does not correlate, therefore, with the theoretical value. It can be deduced that either (i) the energy-transfer mechanism is not dipole—dipole but some kind of through-bond interaction requiring orbital overlap or multipole interactions (the latter has been observed for free $Eu^{3+}$ and $Tb^{3+}$ in solution[61]) or (ii) the energy transfer occurs by molecular distortions of the ligand framework in solution, reducing the interlanthanide distance $R$ and hence facilitating more efficient energy transfer. The first case is less likely, on the basis of the poor orbital overlap of the ligand framework presented, as the disulfide bridges between the lanthanide centers act as insulating spacers between the separate ligand $\pi$ systems; the buried nature of the 4f orbitals also somewhat precludes the orbital overlap required for the electron-exchange type energy-transfer mechanism. The second case must lead to the conclusion that an alternative structure where the lanthanide centers are in closer proximity must exist in solution; this alternative structure would therefore be predominantly responsible for the energy-transfer efficiencies observed. When the dihedral bond angles of both C—S—S bonds are set to 104° (as per experimentally observed disulfide bonds)[62] and the rest of the minimization is retained in the configuration calculated for the protracted state (pseudo-*exo*-macrocycle), the result was a pseudo-*endo*-macrocycle with a cis—cis conformation of the disulfide bridges and an interlanthanide distance of 7.8 Å (Figure 8b)

Calculation of the energy-transfer efficiency between the lanthanide centers in the pseudo-*endo*-macrocycle model using values of 7.8 Å for $R$ and 9.0 Å for $R_0$ with eq 2 leads to a value of $\eta$ = 70%. This efficiency is very similar to the value calculated experimentally for the $\mathbf{EuTbL^x_2}$ macrocycle ($\eta$ = 66%). It is therefore a strong possibility that energy transfer occurs predominantly through the proposed pseudo-*endo* state of the macrocycle, via a dipole—dipole mechanism. The interlanthanide energy transfer leading to the quenching of the Tb excited state is then a result of a dynamic exchange of the macrocycle conformations. The efficiency of energy transfer observed in $\mathbf{EuTbL^x_2}$, in our case, is lower than in the heterometallic lanthanide helicates developed by Piguet and Bünzli and co-workers,[17,58] which display superior energy-transfer yields of 72% and 82%, due to through-bond energy-transfer contributions from the extended conjugation of the $\pi$-orbitals in these systems. Additionally, in these systems the interlanthanide distance is dictated by the ligand binding-site geometry.

## CONCLUSION

We have synthesized and characterized a novel and versatile ligand, $\mathbf{H_3L^x}$, based on the DTPA-bis(amide) motif for lanthanide(III) complexation incorporating thiol pendant arms that can be used in further work for biological or surface-binding applications. Our versatile ligand design ($\mathbf{H_3L^x}$) and the use of activated thiol chemistry ($\mathbf{H_3L^y}$) enabled us to produce a new bimetallic photoactive molecule ($\mathbf{EuTbL^x_2}$) from monofunctional photoactive building blocks. The $\mathbf{EuTbL^x_2}$ macrocycle displays two-color emission with a weak energy-transfer process operating between the lanthanide centers. The potential of the assembly of mononuclear lanthanide complexes to binuclear systems under mild conditions is currently being explored for the development of multimodal and dual-color probes, opening new possibilities for choosing metals with attractive magnetic or radioactive properties in conjunction with luminescent centers.

## ASSOCIATED CONTENT

**Supporting Information.** Fourteen figures showing NMR spectra of $\mathbf{H_3L^x}$, $\mathbf{H_3L^y}$, and $\mathbf{LaL^x}$; UV—vis absorption spectra of $\mathbf{H_3L^x}$, $\mathbf{H_3L^y}$, and $\mathbf{NdL^x}$; excitation spectra of $\mathbf{NdL^x}$, $\mathbf{YbL^x}$, and $\mathbf{ErL^x}$; emission spectra of statistically formed $\mathbf{EuTbL^x_2}$; and UV—vis absorption spectra monitoring thiol reactivity. This material is available free of charge via the Internet at http://pubs.acs.org.

## AUTHOR INFORMATION

**Corresponding Author**
z.pikramenou@bham.ac.uk

## ACKNOWLEDGMENT

We thank BBSRC (D.J.L.) and EPSRC (M.C.S., P.B.G) for funding of the studentships, together with the School of Chemistry at the University of Birmingham. Some of the spectrometers used in this research were obtained, through Birmingham Science City: Innovative Uses for Advanced Materials in the Modern World (West Midlands Centre for Advanced Materials Project 2), with support from Advantage West Midlands (AWM) and partial funding by the European Regional Development Fund (ERDF).

## REFERENCES

(1) Louie, A. *Chem. Rev.* **2010,** *110,* 3146–3196.
(2) Kuil, J.; Velders, A. H.; van Leeuwen, F. W. B. *Bioconjugate Chem.* **2010,** *21,* 1709–1719.
(3) Alric, C.; Taleb, J.; Le Duc, G.; Mandon, C.; Billotay, C.; Le Meur-Herland, A.; Brochard, T.; Vocanson, F.; Janier, M.; Perriat, P.; Roux, S.; Tillement, O. *J. Am. Chem. Soc.* **2008,** *130,* 5908–5915.
(4) Manning, H. C.; Goebel, T.; Thompson, R. C.; Price, R. R.; Lee, H.; Bornhop, D. J. *Bioconjugate Chem.* **2004,** *15,* 1488–1495.
(5) Lewis, D. J.; Bruce, C.; Bohic, S.; Cloetens, P.; Hammond, S. P.; Arbon, D.; Blair-Reid, S.; Pikramenou, Z.; Kysela, B. *Nanomedicine* [Online early access]. DOI: 10.2217/NNM.10.96. Published Online: Sep 29, 2010.
(6) Tremblay, M. S.; Halim, M.; Sames, D. *J. Am. Chem. Soc.* **2007,** *129,* 7570–7577.
(7) Grynkiewicz, G.; Poenie, M.; Tsien, R. Y. *J. Biol. Chem.* **1985,** *6,* 3440–3450.
(8) Howell, R. C.; Spence, K. V. N.; Kahwa, I. A.; White, A. J. P.; Williams, D. J. *Dalton Trans.* **1996,** 961–968.
(9) Bünzli, J.-C. G.; Froidevaux, P.; Harrowfield, J. M. *Inorg. Chem.* **1993,** *32,* 3306–3311.
(10) Canard, G.; Koeller, S.; Bernardinelli, G.; Piguet, C. *J. Am. Chem. Soc.* **2008,** *130,* 1025–1040.
(11) Placidi, M. P.; Villazara, A. J. L.; Natrajan, L. S.; Sykes, D.; Kenwright, A. M.; Faulkner, S. *J. Am. Chem. Soc.* **2009,** *131,* 9916–9917.

(12) Tremblay, M. S.; Sames, D. *Chem. Commun.* **2006,** 4116–4118.
(13) Andre, N.; Jensen, T. B.; Scopelliti, R.; Imbert, D.; Elhabiri, M.; Hopfgartner, G.; Piguet, C.; Bünzli, J.-C. G. *Inorg. Chem.* **2004,** *43,* 515–529.
(14) Costes, J.-P.; Dahan, F.; Dupuis, A.; Lagrave, S.; Laurent, J.-P. *Inorg. Chem.* **1998,** *37,* 153–155.
(15) Costes, J.-P.; Nicodeme, F. *Chem.—Eur. J.* **2002,** *8,* 3442–3447.
(16) Andre, N.; Scopelliti, R.; Hopfgartner, G.; Piguet, C.; Bünzli, J.-C. G. *Chem. Commun.* **2002,** 214–215.
(17) Elhabiri, M.; Scopelliti, R.; Bünzli, J.-C. G.; Piguet, C. *J. Am. Chem. Soc.* **1999,** *121,* 10747–10762.
(18) Ruston, L. L.; Robertson, G. M.; Pikramenou, Z. *Chem.—Asian J.* **2010,** *5,* 571–580.
(19) Castaño-Briones, M. M.; Bassett, A. P.; Meason, L. L.; Ashton, P. R.; Pikramenou, Z. *Chem. Commun.* **2004,** 2832–2833.
(20) Glover, P. B.; Ashton, P. R.; Childs, L. J.; Rodger, A.; Kercher, M.; Williams, R. M.; De Cola, L.; Pikramenou, Z. *J. Am. Chem. Soc.* **2003,** *125,* 9918–9919.
(21) Lewis, D. J.; Day, T. M.; MacPherson, J. V.; Pikramenou, Z. *Chem. Commun.* **2006,** 1433–1435.
(22) Demas, J. N.; Crosby, G. A. *J. Phys. Chem.* **1971,** *75,* 991–1024.
(23) Nakamura, K. *Bull. Chem. Soc. Jpn.* **1982,** *55,* 2697.
(24) Meech, S. R.; Phillips, D. *J. Photochem.* **1983,** *23,* 193.
(25) Synergy Software. *Kaleidagraph 3.51,* 2000.
(26) Ciba-Geigy. Bis-Dioxo-Morpholine Derivatives Bis[2,6, Dioxomorpholinyl-(4)]Phenylenes and Alkylenes. United States Patent 3,660,388, 1972.
(27) Wang, Y. M.; Cheng, T. H.; Liu, G. C.; Sheu, R. S. *J. Chem. Soc., Dalton Trans.* **1997,** 833–838.
(28) Jaszberenyi, Z.; Toth, E.; Kalai, T.; Kiraly, R.; Burai, L.; Brucher, E.; Merbach, A. E.; Hideg, K. *J. Chem. Soc., Dalton Trans.* **2005,** 694–701.
(29) Gulgas, C. G.; Reineke, T. M. *Inorg. Chem.* **2005,** *44,* 9829–9836.
(30) Kimpe, K.; Parac-Vogt, T. N.; Laurent, S.; Pierart, C.; Elst, L. V.; Muller, R. N.; Binnemans, K. *Eur. J. Inorg. Chem.* **2003,** 3021–3027.
(31) Botteman, F.; Nicolle, G. M.; Elst, L. V.; Laurent, S.; Merbach, A. E.; Muller, R. N. *Eur. J. Inorg. Chem.* **2002,** 2686–2693.
(32) Parker, D.; Pulukkody, K.; Smith, F. C.; Batsanov, A.; Howard, J. A. K. *J. Chem. Soc., Dalton Trans.* **1994,** 689–693.
(33) Franklin, S. J.; Raymond, K. N. *Inorg. Chem.* **1994,** *33,* 5794–5804.
(34) Konings, M. S.; Dow, W. C.; Love, D. B.; Raymond, K. N.; Quay, S. C.; Rocklage, S. *Inorg. Chem.* **1990,** *29,* 1488–1491.
(35) Geraldes, C. F. G. C.; Urbano, A. M.; Hoefnagel, M. A.; Peters, J. A. *Inorg. Chem.* **1993,** *32,* 2426–2432.
(36) Barton, D. H. R.; Chen, C.; Wall, G. M. *Tetrahedron* **1991,** *47,* 6127–6138.
(37) Beckwith, A. L. J.; Duggan, S. A. M. *J. Chem. Soc., Perkin Trans. 2* **1994,** 1509–1518.
(38) Tada, H.; Teranishi, K.; Inubushi, Y.; Ito, S. *Chem. Commun.* **1998,** 2345–2346.
(39) Lammers, H.; Maton, F.; Pubanz, D.; van Lauren, M. W.; van Bekkum, H.; Merbach, A. E.; Muller, R. N.; Peters, J. A. *Inorg. Chem.* **1997,** *36,* 2527–2538.
(40) Murov, S. L.; Carmichael, I.; Hug, G. L. *Handbook of Photochemistry*; Marcel Dekker: New York, 1993.
(41) Carnall, W. T.; Fields, P. R.; Rajnak, K. *J. Chem. Phys.* **1968,** *49,* 4413–4455.
(42) Carnall, W. T.; Fields, P. R.; Wybourne, B. G. *J. Chem. Phys.* **1965,** *42,* 3797–3806.
(43) Holz, R. C.; Chang, C. A.; Horrocks, W. W., Jr. *Inorg. Chem.* **1991,** *30,* 3270–3275.
(44) Wolbers, M. P. O.; van Veggel, F. C. J. M.; Snellink-Ruel, B. H. M.; Hofstraat, J. W.; Geurts, F. A. J.; Reinhoudt, D. N. *J. Chem. Soc., Perkin Trans. 2* **1998,** 2141–2150.
(45) Haas, Y.; Stein, G.; Wurzburg, E. *J. Chem. Phys.* **1974,** *60,* 258–263.
(46) Petoud, S.; Bünzli, J.-C. G.; Glanzman, T.; Piguet, C.; Xiang, Q.; Thummel, R. P. *J. Lumin.* **1999,** *82,* 69–79.
(47) Couchet, J.-M.; Azema, J.; Tisnes, P.; Picard, C. *Inorg. Chem. Commun.* **2003,** *6,* 978–981.
(48) Glover, P. B.; Bassett, A. P.; Nockemann, P.; Kariuki, B. M.; Van Deun, R.; Pikramenou, Z. *Chem.—Eur. J.* **2007,** *13,* 6308–6320.
(49) Bassett, A. P.; Van Deun, R.; Nockemann, P.; Glover, P. B.; Kariuki, B. M.; Van Hecke, K.; Van Meervelt, L.; Pikramenou, Z. *Inorg. Chem.* **2005,** *44,* 6410–6412.
(50) Otto, S.; Furlan, R. L. E.; Sanders, J. K. M. *Science* **2002,** *297,* 590–593.
(51) Ramstrom, O.; Lehn, J.-M. *ChemBioChem* **2000,** *1,* 41–48.
(52) Alam, M. M.; Fujitsuka, M.; Watanabe, A.; Ito, O. *J. Chem. Soc., Perkin Trans. 2* **1998,** 817–824.
(53) Hermanson, G. T. *Bioconjugate Techniques*; Academic Press: San Diego, CA, 1996.
(54) Tam, J. P.; Wu, C. R.; Liu, W.; Zhang, J. W. *J. Am. Chem. Soc.* **1991,** *113,* 6657–6662.
(55) Yu, J. A.; Lessard, R. B.; Bowman, L. E.; Nocera, D. G. *Chem. Phys. Lett.* **1991,** *187,* 263–268.
(56) Shah, J. *Curr. Sci.* **1980,** *49,* 736–738.
(57) Froidevaux, P.; Bünzli, J.-C. G. *J. Phys. Chem.* **1994,** *98,* 532–536.
(58) Piguet, C.; Bünzli, J.-C. G.; Bernardinelli, G.; Hopfgartner, G.; Williams, A. F. *J. Am. Chem. Soc.* **1993,** *115,* 8197.
(59) Horrocks, W. W., Jr.; Rhee, M.-J.; Snyder, A. P.; Sudnick, D. R. *J. Am. Chem. Soc.* **1980,** *102,* 3650–3652.
(60) Allinger, N. L. *J. Am. Chem. Soc.* **1977,** *99,* 8127–8134.
(61) Chrysochoos, J. *J. Lumin.* **1974,** *9,* 79–93.
(62) Van Wart, H. E.; Lewis, A.; Scheraga, H. A.; Saeva, F. D. *Proc. Natl. Acad. Sci. U.S.A.* **1973,** *70,* 2619–2623.